5 Production and Spectroscopy of Antihydrogen

C. Amsler, A. Glauser, O. Iannarelli, D. Lindelöf, N. Madsen, H. Pruys, and C. Regenfus

in collaboration with:
CERN, University of Aarhus, Brescia, Genoa, Pavia, Rio de Janeiro, Swansea, Tokyo

(ATHENA Collaboration)

The final goal of the ATHENA experiment is a test of the CPT symmetry in the baryon and lepton sectors by comparing the energy levels of antihydrogen and hydrogen atoms. The long lifetime (122 ms) of the metastable (anti-) hydrogen 2s level is associated with a relative natural line width of 5×10^{-16} for the 1s-2s transition, which can be exploited by two-photon laser spectroscopy. Such high precision measurements would also give valuable experimental information on the gravitational interaction of antihydrogen, because a change in the 1s-2s transition frequency could also originate from a different redshift of antihydrogen and hydrogen atoms in the gravitational field of the earth.

Antihydrogen forms when antiprotons are mixed with cold positrons. In 2001-2002 we demonstrated trapping, cooling and transfer of $\sim 10^4$ cold antiprotons into the mixing trap. In the positron accumulator 150 million positrons were routinely accumulated within 5 minutes. Excellent vacuum conditions could be maintained during and after the transfer process, with a lifetime of antiprotons and positrons exceeding several hours. In 2002 we demonstrated for the first time the production of cold antihydrogen atoms in large quantities [1]. The observation of antihydrogen through its annihilation was achieved with the high granularity detector built in our institute. These results were obtained following improvements to the apparatus, in particular a more efficient positron transfer, the implementation of non-destructive plasma diagnostics, and better signal-to-noise ratio for 511 keV photon detection.

Antihydrogen was produced with $\bar{p}e^+$ mixing cycles of about 3 minutes duration which could be repeated every 500 seconds thanks to our fast positron accumulator. At the beginning of each mixing cycle about 10'000 $\bar{p}$ with kinetic energy of $\sim$ 50 eV entered a large and dense positron plasma of typically 70 million e^+. Rapid cooling of the antiprotons in less than 100 msec was observed and the antihydrogen detector registered a rapid increase in the annihilation rate. From the analysis of several hundred cycles a clear signal was identified from unconfined neutral antihydrogen atoms hitting the trap wall. The antihydrogen signal disappeared when the positron plasma was heated to 3500 K.

We refer to previous annual reports and to the experimental proposal [2] for details on the apparatus.

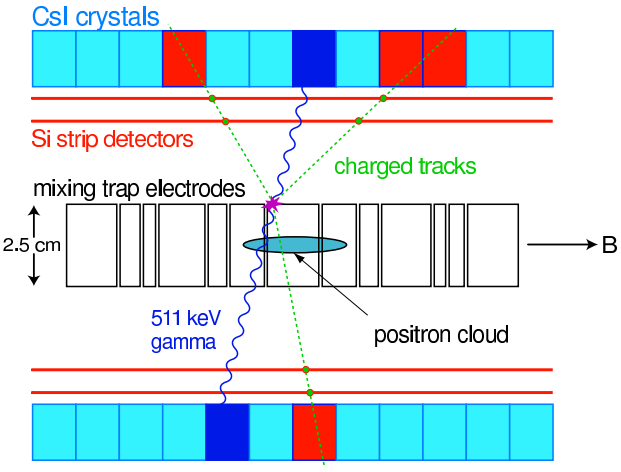

Figure 5.1: *Principle of antihydrogen detection (see text).*

5.1 Development of the antihydrogen detector

The detector (fig. 5.1) features two cylindrical layers of double-sided silicon microstrips (8192 channels) and 16 rows of 12 pure CsI crystals ($17 \times 13 \times 17.5$ mm^3) read out by avalanche photodiodes. It is located in the small space between the (37 mm diameter) UHV vessel of the combination trap and the (70 mm diameter) cold bore of the 3 T superconducting magnet, where vacuum conditions of 10^{-7} mbar and a temperature of 140 K prevail.

The antiproton and positron cease to be confined in the combination trap once bound to antihydrogen. The antiatom therefore collides after less than 1 μs with the surface of the trap electrode. On average three charged pions and three high energy (50-500 MeV) photons are produced by the annihilation of the antiproton, while the positron annihilates with an electron, generating two back-to-back 511 keV photons. The unique identification of antihydrogen is based on the 180° opening angle between the two 511 keV photons, as seen from the antiproton annihilation vertex. A 5μs timing coincidence between the detection of the pions and two 511 keV photons is also required.

Pure CsI was chosen because of the excellent light yield at low temperature (50'000 photons/MeV at 80 K [3]), together with a total absorption probability of 20% for 511 keV photons. Initially, the crystals were coupled to pn photodiodes, but the quantum efficiency decreased dramatically below 450 nm, especially at low temperatures. A systematic study of this effect was undertaken by building an optical spectrometer based on an Echelette grating (fig. 5.2) [4]. The selected light (resolution of

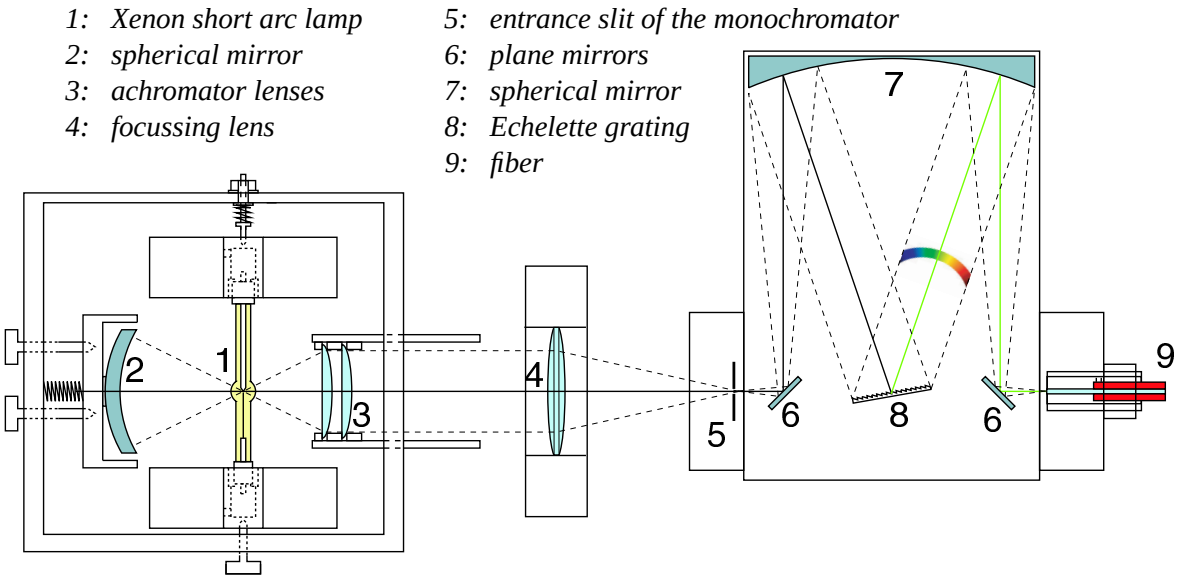

Figure 5.2: *Optical spectrometer (after [4]).*

2 nm FWHM) exiting the spectrometer was transferred by an optical fiber to a liquid nitrogen cell containing the test photodiodes. Figure 5.3 shows the relative quantum efficieny as a function of temperature and wavelength (a unit relative efficiency corresponds to an absolute efficiency of 62%, obtained by comparison with a commercially calibrated photodiode). One observes a fast drop in the detection efficiency of blue light with decreasing temperature. The reason for this behaviour is not quite understood. In addition, the performance of our photodiodes deteriorated with time (apparently due to corrosion from the iodine in CsI). In 2002 we therefore replaced all photodiodes by avalanche photodiodes (APD) which have the advantage of a large gain and hence a much better signal-over-noise ratio. Figure 5.4 shows a photograph of one of the 300 APD's purchased from CMS (a small batch from their 160'000 supply!). The gain of the APD as a function of bias voltage was measured

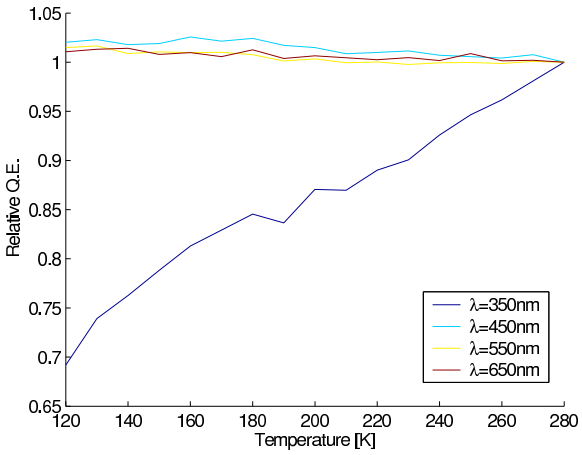

Figure 5.3: *Relative quantum efficiency of a photodiode as a function of temperature and wavelength.*

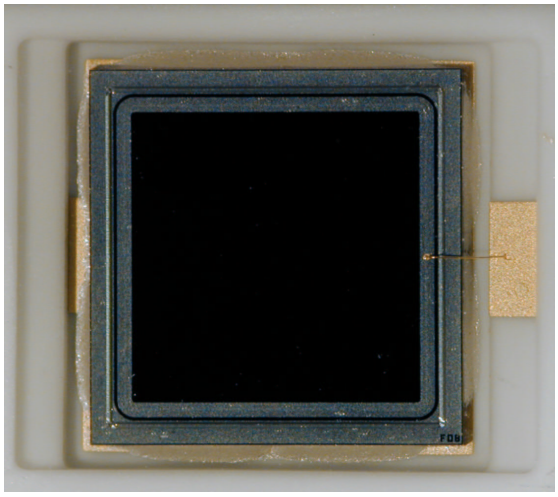

Figure 5.4: *Avalanche photodiode (5×5 mm^2) purchased from the CMS experiment. The epoxy window was removed with sulfuric acid.*

with a pulsed light emitting photodiode (fig. 5.5). The plateau at low voltage corresponds to unit gain, the rise is due to the generated avalanche in the diode. The voltage at which multiplication starts depends on temperature, due to mobility which is a function of temperature. The advantage of APD's for ATHENA is the very low dark current at low temperature, so that the signal can be amplified to very high values. We settled for a gain of 20 corresponding to a signal-over-noise ratio of about 100.

The detector is now working to our full satisfaction. Figure 5.6 shows the measured photon energy spectrum with APDs from positron annihilation in the combination trap, summed over all crystals. The peak at 511 keV has a resolution of 18% FWHM and is well separated from the Compton plateau and the noise.

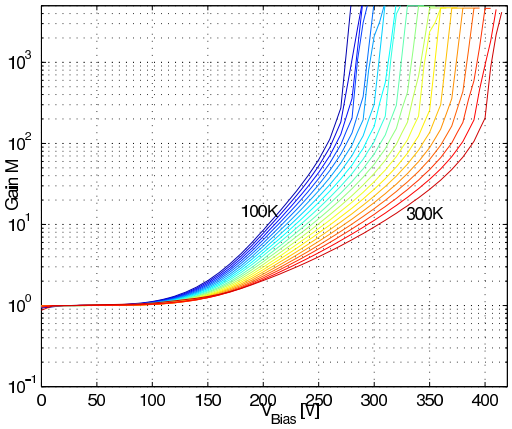

Figure 5.5: *Gain of an avalanche photodiode as a function of bias voltage V for different temperatures. The curves are fits with exponential functions of the form* $a + b\exp(cV)$.

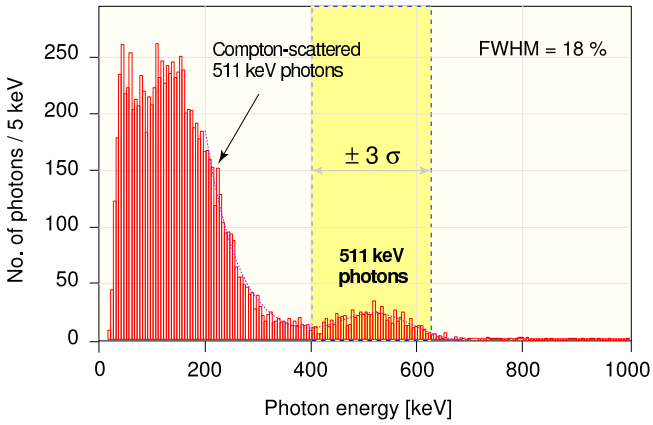

Figure 5.6: *Measured photon energy distribution for positron annihilation in the combination trap (sum over all 192 crystals).*

5.2 Positron heating

Characteristics of the positron plasma such as shape, dimension, density and temperature, are important parameters for the antiproton-positron interaction. For instance, the temperature dependence of antihydrogen formation depends crucially on the formation mechanism, spontaneous radiative transitions (which populates the lower energy levels) or three-body combination (which populates the higher energy states).

The positron plasma is confined in the central part of the mixing trap by the harmonic axial potential. The positrons cool to the ambient temperature of the surrounding trap walls ($\simeq$ 15 K) through synchrotron radiation in the 3 T magnetic field, with a typical time constant of 400 msec. The shape of the plasma is a prolate ellipsoid, 3 cm long and 4 mm in diameter, with a density of $2.5\times\ 10^8$ cm^{-3}. We use a non-destructive diagnostic to control and monitor the positron plasma parameters. It is based on the excitation of the first two axial resonant plasma oscillation modes (dipole, quadrupole) by applying a sinusoidal perturbation to one electrode, and then observing the induced current in a pick-up electrode [5]. The plasma density and shape of the plasma is extracted from the measured frequencies of the dipole and quadrupole modes [6]. By applying an RF signal to one of the trap electrodes that sweeps a frequency band near the dipole frequency (21 MHz), the plasma can be heated in a controlled way, depending on the heating amplitude of typically a few mV. Antihydrogen formation can therefore be controlled and even quenched by controlling the positron plasma temperature. The dependence of the plasma temperature shift ΔT on the excitation voltage V_d was measured and is shown in fig. 5.7.

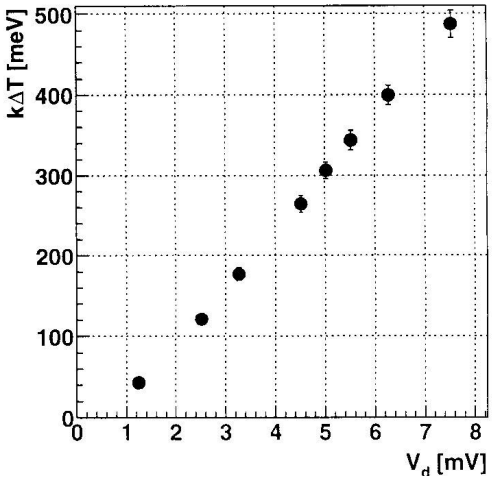

Figure 5.7: *Plasma temperature variation ΔT vs. RF heating amplitude V_d.*

5.3 Antihydrogen production

A positron-antiproton mixing cycle lasts for 500 s and starts with the transfer of about $7\ \times\ 10^7$ positrons into the combination trap, where they cool to $\simeq$ 15 K. A W-shaped potential (nested trap) is then formed around the positron plasma. Positrons are confined in the central part of the potential. Simultaneously, 10'000 antiprotons are captured, cooled by electrons in the capture trap and then launched into the combination trap. The antiproton and the positron plasma mix for about 3 minutes, after which all particles are dumped and the process is repeated.

Positron cooling of antiprotons was reported earlier by the ATRAP collaboration [7]. In ATHENA, we studied this process with 10'000 antiprotons crossing a much larger and denser positron plasma. Antiprotons were stored in a side potential well and then launched into the mixing region with a kinetic energy of $\simeq$ 50 eV. Antiprotons traversing the positron plasma loose energy through collisions. Evidence for positron cooling was obtained by lowering the potentials of the side wells in the nested trap and measuring the number of annihilating antiprotons as a function of voltage. The results show that, after a short initial cooling time of $\simeq$ 500 ms, the two plasmas separate both in longitudinal and radial direction, leading to a decreasing overlap and hence interaction between the two antiparticle species.

Annihilation events trigger the silicon detector. In the offline analysis antiproton annihilation vertices are reconstructed from the silicon detector data. For each reconstructed vertex, we search for two well separated 511 keV photon hits in the crystal data. To search for antihydrogen events we calculate the opening angle $\Theta_{\gamma\gamma}$, between the γ-directions. For an antihydrogen event, this angle should be 180°.

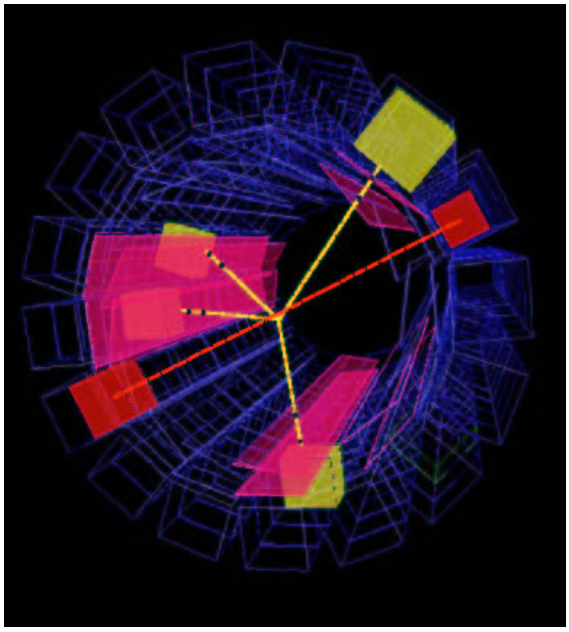

Figure 5.8: *Reconstructed antihydrogen annihilation event with four charged particles from a common vertex, and two isolated 511 keV photons that appear back-to-back when looking from the vertex.*

Figure 5.8 shows an event compatible with antihydrogen annihilation.The spatial resolution on the annihilation vertex is mainly determined by the unknown track curvature in the 3 T magnetic field. The charged particle vertex resolution in radial direction was measured experimentally by letting antiprotons annihilate on the trap electrodes (radius 12.5 mm). The measured distribution agrees well with the Monte Carlo prediction and the radial resolution is $\sigma \simeq 4$ mm. The simulation gives a probability of 50 % for vertex reconstruction, in agreement with measurement. This probability is determined by the solid angle of the outer silicon layer and the trigger and detector efficiencies. The interaction probability of 511 keV photons in a crystal is about 20 %. Taking into account the solid angle of the CsI calorimeter, crystal inefficiencies and all cuts, the detection efficiency for both photons is about 1 %, leading to a total efficiency for event reconstruction of about 0.5 %.

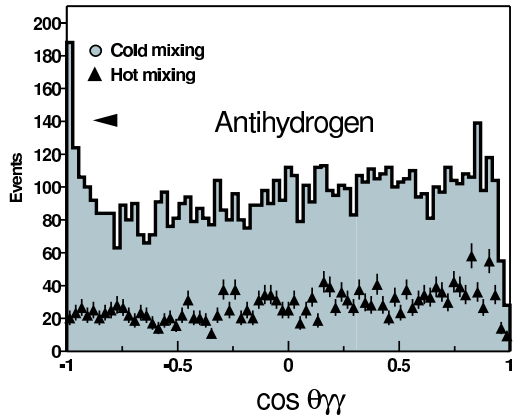

The histogram shows cold mixing data (7'125 events). The triangles represent hot mixing data, scaled by 1.6 to the same number of mixing cycles (from ref. [1]).

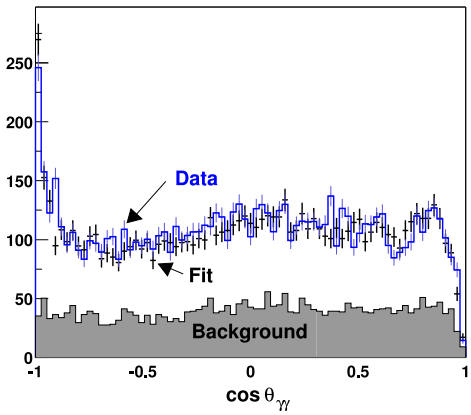

Fit to the opening angle distribution for cold mixing using simulated data for antihydrogen annihilation and antiproton background from hot mixing (for a slightly larger data sample).

Figure 5.9: *Distributions of the opening angle* $\Theta_{\gamma\gamma}$.

Figure 5.9 shows the opening angle distribution from 165 mixing cycles of antiprotons with cold positrons. The peak at cos $\Theta_{\gamma\gamma}$ = -1 is clearly observed. It contains 131 $\pm$ 22 events, corresponding

to a statistical significance of more than 5σ. The triangles in fig. 5.9 (left) represent hot mixing data in which no antihydrogen formation is expected. The flat background from spatially uncorrelated two-photon events is due to high-energy photons from antiproton annihilations on the wall, producing electromagnetic showers with secondary positrons. This process does not produce a peak at 180 °.

We have studied the relative contribution of antihydrogen and antiproton annihilations. Antihydrogen atoms annihilate on a trap electrode. On the other hand, antiprotons are confined by the fields and oscillate in the centre of the trap, where they may annihilate with rest gas or with positive ions trapped with the positron plasma. We have measured the $(x - y)$ vertex distribution (fig. 5.10) for antiproton mixing with cold and hot positron plasma. For cold mixing, a clear image of the trap electrodes is obtained, consistent with antihydrogen annihilations on the wall. The distribution for hot mixing, also shown in fig. 5.10, has a very different shape. Antihydrogen production is suppressed, and stored antiprotons annihilate with trapped ions (or with rest gas) in the centre of the trap. The relative contribution of antihydrogen versus antiproton background in the cold mixing data was determined by fitting the $x - y$ distribution with a simple model consisting of two contributions, (i) antihydrogen annihilation on the trap wall (from Monte Carlo simulation) and (ii) antiproton-ion annihilation inside the trap volume (from the hot mixing measurement). The fit gave a relative contribution of 35 $\pm$ 10% background in fig. 5.9. The same result is obtained by fitting the $\Theta_{\gamma\gamma}$ distributions for hot and cold mixing. The result is shown in fig. 5.9 (right). Hence about 65 % of the events in the $\Theta_{\gamma\gamma}$ distribution are actually due to antihydrogen formation, where at least one of the two 511 keV γ's stems from background. The data collected in 2002 correspond to the production of about 10^6 antihydrogen atoms in the ATHENA apparatus. Figure 5.11 shows the number of reconstructed vertices as a function of time during a typical mixing cycle. Immediately after antiproton injection a sharp increase in the number of annihilations is observed by the detector. The event rate is above 100 Hz during the first second. The annihilation rate then decreases slowly to 1 Hz after 3 minutes. Fast cooling antiprotons within the positron cloud lead to a high initial antihydrogen rate. As most of their kinetic energy is lost the remaining antiprotons are located in the side wells or are radially separated from the positron plasma, thus reducing the probability of antihydrogen formation.

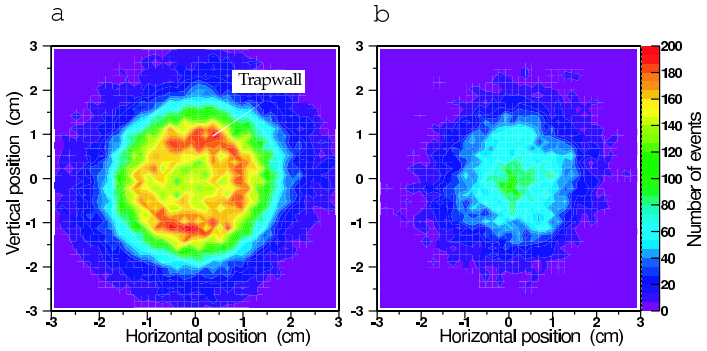

Figure 5.10: *Transverse vertex positions for mixing with cold positrons (left) and hot positrons (right) (from ref. [1]).*

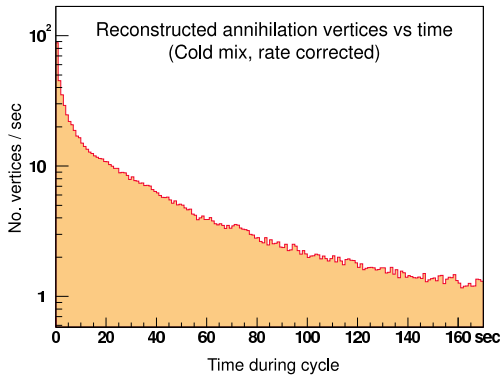

Figure 5.11: *Number of reconstructed annihilation vertices as a function of time after injection of the antiprotons into the positron plasma.*

We studied also the temperature dependence of antihydrogen production. The distributions show that for increasing plasma temperature, the relative size of the back-to-back peak decreases and there is clear evidence that antihydrogen production takes place even at room temperature (30 meV). This speaks in favour of radiative combination as the dominant formation mechanism, since three-body combination is only expected to occur at very low temperatures (much below 10 meV). Furthermore the temperature dependence of antihydrogen production seems to follow the simple $1/T$ dependence consistent with radiative combination. These are very good news for atomic level spectroscopy, since we will require antihydrogen to be in the 1s state.

The dependence on temperature can be used for pulsed antihydrogen production. By switching on the RF heating of positrons, antihydrogen production can be switched off within $\sim$ 100 ms. The positron plasma then cools down by synchrotron radiation after switching the RF heating off, and antihydrogen production resumes within less than 1 second (fig. 5.12).

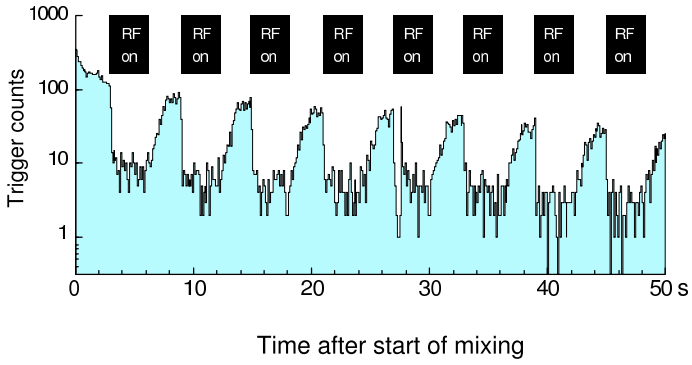

Figure 5.12: *Annihilation trigger rate with and without RF heating of the plasma during 3s intervals.*

5.4 R & D for laser spectroscopy

Until the one year accelerator shutdown in 2005 we will study antihydrogen production and its dependence on parameters such as the number, density and temperature of antiprotons and positrons. Currently roughly 15-20 % of all antiprotons in the mixing trap form antihydrogen, and we are studying ways to increase this number. Stimulated combination by irradiation with laser light is also being investigated.

In 2002 the Zurich group initiated the first part of the spectroscopy phase, the construction of a laser system to generate the 243 nm light for 1s-2s two-photon spectroscopy in antihydrogen [8]. No laser-sources are available in the ultra-violet region. We therefore use a non-linear technique to generate the 243 nm light from a laser source of longer wavelength. Figure 5.13 shows schematically the laser system that is currently being implemented [8]. Most of the equipment was provided by the University of Aarhus. The system consists first of a Coherent Innova Sabre - Kr^+ ion laser that emits 4 W in the range 406 nm to 415 nm. The Kr^+ ion laser pumps a Coherent 899-21 Ring Dye laser that circulates Coumarin 102 dye which emits in the range 460 nm to 516 nm. The dye laser is necessary to introduce tunability in the system, as an ion laser emits only at specific wavelengths. The dye laser is tuned to a wavelength of 486.2 nm which is twice the wavelength of the two-photon 1s-2s transition in antihydrogen. About 500 mW of light is emitted at 486.2 nm.

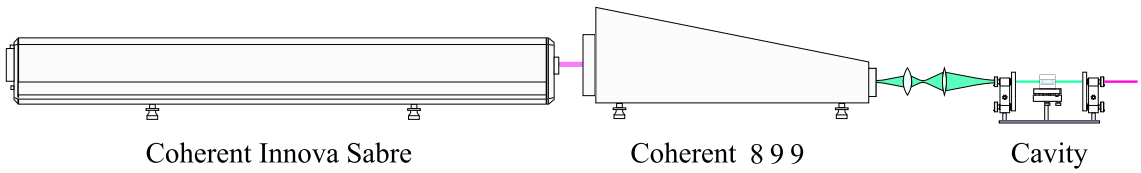

Figure 5.13: *Sketch of the laser chain to generate the 243 nm light for 1s-2s two-photon spectroscopy.*

The light from the dye laser is sent into an external frequency doubling cavity containing a nonlinear crystal. The second harmonic generation power in the crystal is maximum when the refractive indices n for the fundamental and the second harmonics are equal. Since the refractive index depends on frequency, a birefringent crystal with a suitably oriented optical axis is used, in which the ordinary ray is chosen for the fundamental frequency and the extraordinary ray for the second harmonic, i.e. $n_o(\omega) = n_e(2\omega)$. Losses are reduced by using a crystal cut such that the light with fundamental frequency traversing the crystal penetrates the crystal under the Brewster angle. Under this angle the polarisation parallel to the plane formed by the incident beam and the normal to the crystal surface is not reflected but transmitted into the crystal. The cavity that was chosen is shown in fig. 5.14 (for details see ref. [8]). It consists of a Brewster cut rhomb shaped beta barium borate (BBO) crystal with a side length of 8 mm. The light from the dye laser enters from the right. The convex mirrors have a reflection coefficient of 100% for the first harmonic and a transmission coefficient of 95 % for the second harmonic. The locking beam is sent to a photodiode for frequency locking. The external cavity is expected to deliver about 50 mW of laser light at 243.1 nm. In 2002 we installed the clean room and most of the laser system. The various components such as mirrors and the BBO crystal have been purchased. The cavity assembly is close to completion. The setting up of the dye laser was complicated by technical problems. Its operation is now stable but only at about half the nominal power. This is sufficient for the first tests of the frequency doubling, which we expect to commence shortly.

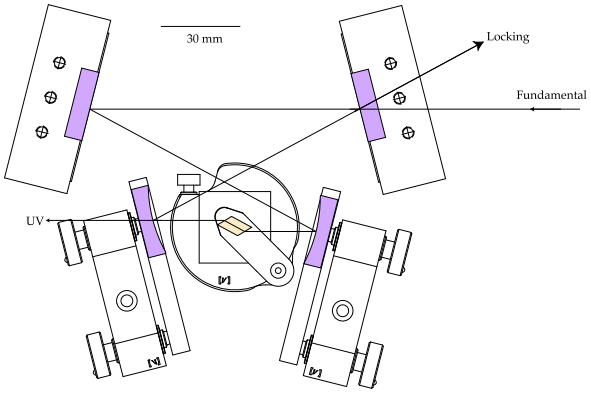

Figure 5.14: *External cavity with BBO crystal (yellow) for second harmonic generation (see text).*

[1] M. Amoretti *et al.*, Nature **419** (2002) 456.

[2] ATHENA proposal, M.H. Holzscheiter et al., CERN-SPSLC/P302, October 1996, see also http://www.cern.ch/athena/.

[3] C. Amsler *et al.*, Nucl. Instr. Meth. in Phys. Res. **A 480** (2002) 494.

[4] A. Glauser, Diplomarbeit, Universität Zürich, 2003.

[5] M. Amoretti *et al.*, submitted to Phys. Rev. Lett.

[6] D. H. E. Dubin, Phys. Rev. Lett. **66** (1991) 2076.

[7] G. Gabrielse *et al.*, Phys. Lett. **B 507** (2001) 1.

[8] O. Iannarelli, Diplomarbeit, Universität Zürich, in preparation.